



# Comprehensive Analysis of *C. glutamicum* Anaplerotic Deletion Mutants Under Defined D-Glucose Conditions

Jannick Kappelmann<sup>1</sup>, Bianca Klein<sup>1</sup>, Mathias Papenfuß<sup>2</sup>, Julian Lange<sup>3</sup>,  
Bastian Blombach<sup>4</sup>, Ralf Takors<sup>3</sup>, Wolfgang Wiechert<sup>1</sup>, Tino Polen<sup>1</sup> and Stephan Noack<sup>1\*</sup>

<sup>1</sup> Institute of Bio- and Geosciences 1, IBG-1: Biotechnology, Forschungszentrum Jülich GmbH, Jülich, Germany, <sup>2</sup> Institute of Biochemical Engineering, Braunschweig University of Technology, Braunschweig, Germany, <sup>3</sup> Institute of Biochemical Engineering, University of Stuttgart, Stuttgart, Germany, <sup>4</sup> Microbial Biotechnology, Campus Straubing for Biotechnology and Sustainability, Technical University of Munich, Straubing, Germany

## OPEN ACCESS

### Edited by:

Yu Wang,  
Chinese Academy of Sciences, China

### Reviewed by:

Guoqiang Xu,  
Jiangnan University, China  
Chen Yang,  
Chinese Academy of Sciences  
(CAS), China

### \*Correspondence:

Stephan Noack  
s.noack@fz-juelich.de

### Specialty section:

This article was submitted to  
Synthetic Biology,  
a section of the journal  
*Frontiers in Bioengineering and  
Biotechnology*

**Received:** 04 September 2020

**Accepted:** 17 December 2020

**Published:** 20 January 2021

### Citation:

Kappelmann J, Klein B, Papenfuß M, Lange J, Blombach B, Takors R, Wiechert W, Polen T and Noack S (2021) Comprehensive Analysis of *C. glutamicum* Anaplerotic Deletion Mutants Under Defined D-Glucose Conditions. *Front. Bioeng. Biotechnol.* 8:602936.  
doi: 10.3389/fbioe.2020.602936

Wild-type *C. glutamicum* ATCC 13032 is known to possess two enzymes with anaplerotic (C4-directed) carboxylation activity, namely phosphoenolpyruvate carboxylase (PEPCx) and pyruvate carboxylase (PCx). On the other hand, C3-directed decarboxylation can be catalyzed by the three enzymes phosphoenolpyruvate carboxykinase (PEPCK), oxaloacetate decarboxylase (ODx), and malic enzyme (ME). The resulting high metabolic flexibility at the anaplerotic node compromises the unambiguous determination of its carbon and energy flux in *C. glutamicum* wild type. To circumvent this problem we performed a comprehensive analysis of selected single or double deletion mutants in the anaplerosis of wild-type *C. glutamicum* under defined D-glucose conditions. By applying well-controlled lab-scale bioreactor experiments in combination with untargeted proteomics, quantitative metabolomics and whole-genome sequencing hitherto unknown, and sometimes counter-intuitive, genotype-phenotype relationships in these mutants could be unraveled. In comparison to the wild type the four mutants *C. glutamicum* Δpyc, *C. glutamicum* Δpyc Δodx, *C. glutamicum* Δppc Δpyc, and *C. glutamicum* Δpck showed lowered specific growth rates and D-glucose uptake rates, underlining the importance of PCx and PEPCK activity for a balanced carbon and energy flux at the anaplerotic node. Most interestingly, the strain *C. glutamicum* Δppc Δpyc could be evolved to grow on D-glucose as the only source of carbon and energy, whereas this combination was previously considered lethal. The prevented anaplerotic carboxylation activity of PEPCx and PCx was found in the evolved strain to be compensated by an up-regulation of the glyoxylate shunt, potentially in combination with the 2-methylcitrate cycle.

**Keywords:** *Corynebacterium glutamicum*, anaplerosis, phosphoenolpyruvate carboxylase, pyruvate carboxylase, phosphoenolpyruvate carboxykinase, oxaloacetate decarboxylase, malic enzyme, methylcitrate cycle

## INTRODUCTION

*C. glutamicum* is one of the most important organisms for industrial biotechnology and the current product spectrum that is accessible with this host comprises proteinogenic as well as non-proteinogenic amino acids, organic acids, diamines, vitamins, aromates, and alcohols (Becker et al., 2018; Kogure and Inui, 2018). Most production strains have been generated by classical mutagenesis and selection, as well as by targeted and evolutionary metabolic engineering approaches (Lee and Wendisch, 2017; Stella et al., 2019). With the aim to enhance predictability of cellular functions and to reduce interference with heterologous pathways new chassis strains were introduced (Baumgart et al., 2013, 2018; Unthan et al., 2015). Several targeted and untargeted proteomics methods were developed, enabling relative, and absolute quantification of cytosolic as well as membrane-bound proteins (Fränzel et al., 2009; Voges and Noack, 2012; Trötschel et al., 2013; Kübel et al., 2014; Voges et al., 2015; Noack et al., 2017).

At the phosphoenolpyruvate-pyruvate-oxaloacetate node *C. glutamicum* ATCC 13032 (wild type) is known to possess two enzymes with anaplerotic (C4-directed) carboxylation activity, namely phosphoenolpyruvate carboxylase (PEPCx) and pyruvate carboxylase (PCx). On the other hand, C3-directed decarboxylation can be catalyzed by the three enzymes phosphoenolpyruvate carboxykinase (PEPCk), oxaloacetate decarboxylase (ODx), and malic enzyme (ME). While all enzymes show *in vitro* activity in cells grown in defined D-glucose media (Cocaign-Bousquet et al., 1996; Uy et al., 1999; Klaffl and Eikmanns, 2010; Blombach et al., 2013), only PEPCx and PCx are currently considered as dependent essential anaplerotic enzymes under these conditions (Figure 1).

Recently, the anaplerotic node of *C. glutamicum*, which represents a very flexible knot for diverting the carbon and energy flux introduced by different potential substrates, has again attracted our attention. Following detailed mathematical modeling and computational analyses, we could prove that only certain anaplerotic deletion mutants allow to uniquely determine the anaplerotic fluxes (Kappelmann et al., 2016).

Following shake flask experiments, it was shown that a single inactivation of either PEPCx, PCx, ODx or ME in wild-type *C. glutamicum* has no effect on biomass growth (Peters-Wendisch et al., 1993, 1998; Gourdon et al., 2000; Klaffl and Eikmanns, 2010). The only exception was found for PEPCk, whose inactivation resulted in a lower growth rate (Riedel et al., 2001). In contrast, the combined removal of PEPCx and PCx is thought to be lethal for *C. glutamicum* when grown under glycolytic conditions as no other carboxylation reaction enables replenishment of tricarboxylic acid intermediates (Peters-Wendisch et al., 1998). Recently, Schwentner et al. were able to evolve *C. glutamicum* Δ $ppc$  Δ $pyc$  to grow on CGXII medium with 20 g L<sup>-1</sup> D-glucose and 1 g L<sup>-1</sup> yeast extract (or alternatively 1 mM L-glutamate) (Schwentner et al., 2018). Comparative whole-genome sequencing revealed isocitrate dehydrogenase (ICD) as consistent target and the identified mutations could be linked to diminished ICD activities as well as increased activities of the glyoxylate shunt enzymes isocitrate lyase (ICL) and malate

synthase (MS). Operation of the glyoxylate shunt can substitute for the missing carboxylation reactions to replenish oxaloacetate required for growth. Interestingly, on pure D-glucose media this evolution failed in the study reported (Schwentner et al., 2018).

In our study, we performed a comprehensive analysis of selected single or double deletion mutants in the anaplerosis of wild-type *C. glutamicum* under defined D-glucose conditions without other carbon supplements. By applying well-controlled lab-scale bioreactor experiments in combination with untargeted proteomics, quantitative metabolomics and whole-genome sequencing hitherto unknown genotype-phenotype relationships in these mutants could be unraveled and these are discussed in detail with regard to published data.

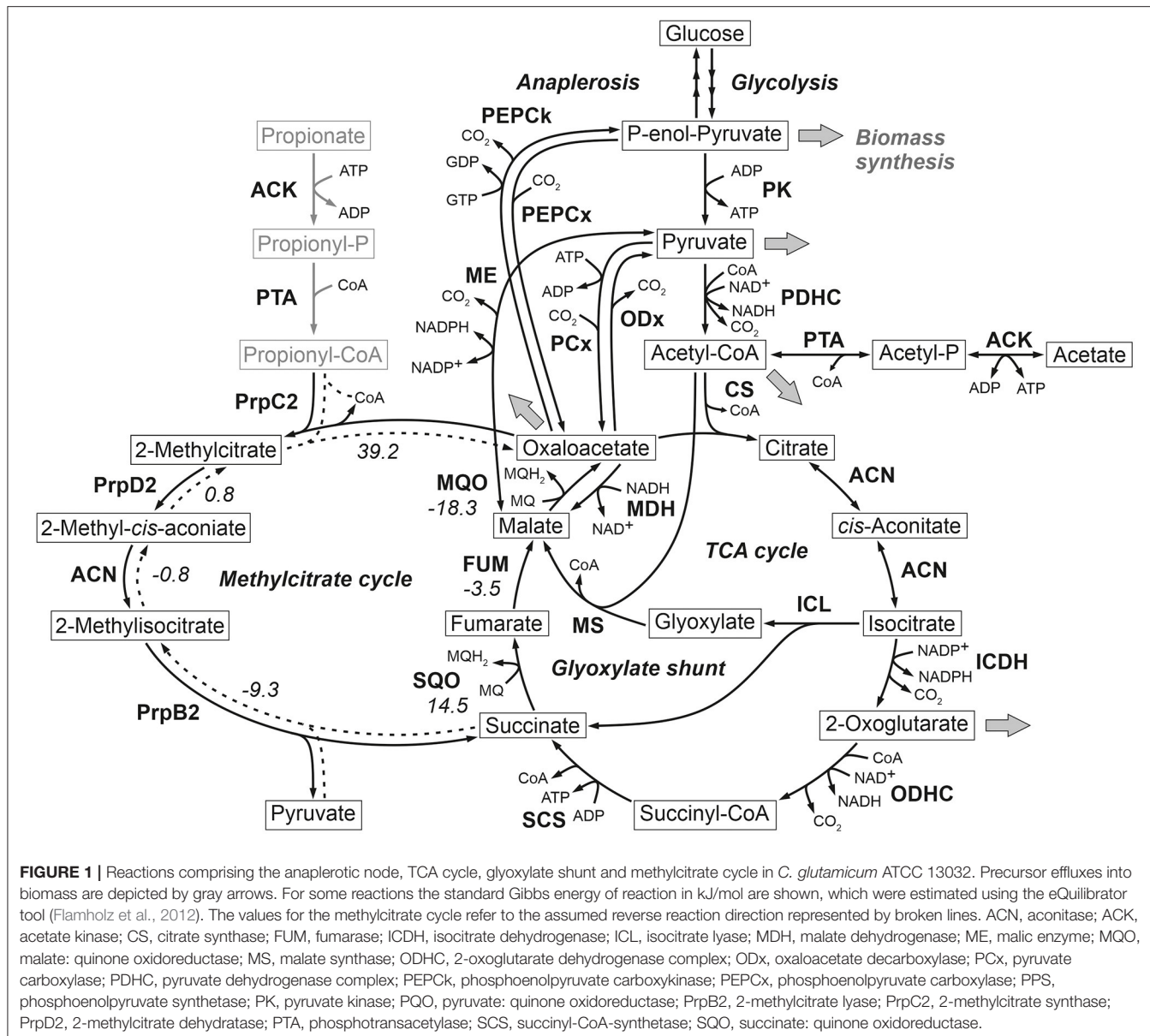
## MATERIALS AND METHODS

### Bacterial Strains

All strains, plasmids and oligonucleotids used in this study are listed in Table 1. The *C. glutamicum* WT as well as the single deletion mutants Δ $pyc$ , Δ $malE$ , Δ $pck$  are from Blombach et al. (2013). The double deletion mutant Δ $ppc$  Δ $pyc$  is described in Schwentner et al. (2018). The three remaining double deletion mutants Δ $pyc$  Δ $odx$ , Δ $ppc$  Δ $malE$  and Δ $pck$  Δ $malE$  were constructed by chromosomal inactivation of the ODx gene  $odx$  in *C. glutamicum* Δ $pyc$ , as well as the ME gene  $malE$  in *C. glutamicum* Δ $pck$  and *C. glutamicum* Δ $ppc$  using the plasmids pK19mobsacB-Δ $odx$  and pK19mobsacB-Δ $malE$ . Isolation of plasmids from *Escherichia coli* was performed as described elsewhere (Eikmanns et al., 1994). Plasmid DNA transfer into *C. glutamicum* was carried out by electroporation and recombinant strains were selected on Luria-Bertani Brain Heart Infusion agar plates containing appropriate concentrations of kanamycin (50 µg mL<sup>-1</sup>) (Van Der Rest et al., 1999). The replacement at the chromosomal locus was verified by colony-PCR using primers  $odxfow$ / $odxrev$  and  $Co-malE1$ / $Co-malE1$ , respectively (Klaffl and Eikmanns, 2010; Blombach et al., 2011). Subsequently, shaking flasks with CGXII preculture medium containing 1% D-glucose (w v<sup>-1</sup>) were inoculated with the corresponding strains (Unthan et al., 2014). Each culture was harvested during the late exponential phase following centrifugation at 4,500 rpm for 10 min, resuspension in sterile saline and finally in 20% (v v<sup>-1</sup>) glycerol solution in sterile 0.9% (w v<sup>-1</sup>) NaCl in distilled water. From this solution cryo stocks were prepared and immediately stored at -80°C. The Δ $ppc$  Δ $pyc$  mutant was able to grow on acetate, from which a corresponding cryo-culture was produced.

### Evolution and Whole-Genome Sequencing of *C. glutamicum* Δ $ppc$ Δ $pyc$

*C. glutamicum* Δ $ppc$  Δ $pyc$  was grown in microtiter plates in a BioLector parallel cultivation system (m2p-labs). Flowerplates with optodes for optical pH and dissolved oxygen (DO) measurements were employed. A cryo-culture for inoculation was washed once with sterile saline and resuspended in D-glucose-free CGXII medium. From this inoculum 50 µL were transferred into each well containing 950 µL 1% D-glucose



medium. The plates were steriley sealed and incubated at 30°C at 1,300 rpm.

For whole-genome sequencing, 200 µL of a well-inoculated at OD<sub>init</sub> = 1 (see **Supplementary Figure 1**) and after growth has ceased was used to inoculate a subsequent shaking flask culture, from which a cryo-culture was produced. From this cryo-culture a sample was generated for whole-genome sequencing using the Illumina platform followed by sequence analysis as described elsewhere (Kranz et al., 2017).

## Bioreactor Cultivations

*C. glutamicum* deletion strains were cultivated in a DASGIP parallel fermentation system (Eppendorf). Bioreactor cultivations of *C. glutamicum* strains were carried out with defined CGXII medium containing 1%

D-glucose and 0.1% undiluted Antifoam 204 but no 3-(N-Morpholino)propanesulfonic acid (MOPS) buffer (Unthan et al., 2014). Bioreactors were inoculated from a preculture in CGXII medium buffered with 42 g L<sup>-1</sup> MOPS at pH 7 which was inoculated directly from a cryo-culture of each strain in 80% 0.9% NaCl/20% glycerol (v v<sup>-1</sup>) stored at -80°C. During bioreactor cultivations DO levels were maintained above 30% by adjusting stirrer speed and oxygen content of the inlet air. The gassing rate was set to 1 vvm and the pH was maintained at pH 7 by feeding either 4 M NaOH or 4 M HCl. The cultivation temperature was 30°C.

For quantitative metabolomics, samples from bioreactor cultivations were drawn into a syringe in technical duplicate at two time points yielding a total of four technical replicates per strain. These time points correspond to target BV

**TABLE 1 |** Strains, plasmids, and oligonucleotides used in this study.

Strains	Relevant characteristic(s) or sequence	Source/reference or purpose
<i>C. glutamicum</i> WT	wild type (WT) strain ATCC 13032, biotin-auxotrophic	American Type Culture Collection
<i>C. glutamicum</i> Δpyc	<i>C. glutamicum</i> WT with deletion of the <i>pyc</i> gene encoding pyruvate carboxylase	Blombach et al., 2013
<i>C. glutamicum</i> ΔmalE	<i>C. glutamicum</i> WT with deletion of the <i>malE</i> gene encoding malic enzyme	Blombach et al., 2013
<i>C. glutamicum</i> Δpck	<i>C. glutamicum</i> WT with deletion of the <i>pck</i> gene encoding phosphoenolpyruvate carboxykinase	Blombach et al., 2013
<i>C. glutamicum</i> Δppc Δpyc	<i>C. glutamicum</i> WT with deletion of the <i>ppc</i> and <i>pyc</i> gene encoding phosphoenolpyruvate carboxylase and pyruvate carboxylase, respectively	Schwentner et al., 2018
<i>C. glutamicum</i> Δpck ΔmalE	<i>C. glutamicum</i> WT with deletion of the <i>pck</i> and <i>malE</i> gene encoding phosphoenolpyruvate carboxykinase and malic enzyme, respectively	This work
<i>C. glutamicum</i> Δpyc Δodx	<i>C. glutamicum</i> WT with deletion of the <i>pyc</i> and <i>odx</i> gene encoding pyruvate carboxylase and oxaloacetate decarboxylase, respectively	This work
<i>C. glutamicum</i> Δppc ΔmalE	<i>C. glutamicum</i> WT with deletion of the <i>ppc</i> and <i>malE</i> gene encoding phosphoenolpyruvate carboxylase and malic enzyme, respectively	This work
<b>Plasmids</b>		
pK19mobsacB-ΔmalE	pK19mobsacB carrying a truncated <i>malE</i> gene	Blombach et al., 2011
pK19mobsacB-Δodx	pK19mobsacB carrying the <i>odx</i> gene with internal 679-bp deletion	Klaffl and Eikmanns, 2010
<b>Oligonucleotides</b>		
odxfow	5'-ACCGGCATCAAATTGTGTC-3'	Primer to verify deletion of <i>odx</i>
odxrev	5'-TTGCCTTGAGCACAATGTC-3'	Primer to verify deletion of <i>odx</i>
Co-malE1	5'-CTTCCAGACACGGAACATCAGAG-3'	Primer to verify deletion of <i>malE</i> (Blombach et al., 2011)
Co-malE2	5'-GTGATCCTCCGAGCGTTCC-3'	Primer to verify deletion of <i>malE</i> (Blombach et al., 2011)

concentrations of 5  $\mu\text{L mL}^{-1}$  ( $\text{OD}_{600} = 6.3$ ) and 10  $\mu\text{L mL}^{-1}$  ( $\text{OD}_{600} = 12.5$ ), covering the mid-exponential phase (cmp. **Supplementary Figure 2**). The actual BV concentration in each sample was measured after sampling and used to calculate the extraction volume.

For untargeted proteomics, sampling was performed directly after all quenching samples for the metabolome analysis had been taken. From each reactor samples were drawn in technical quintuplicate by centrifuging 10 mL of culture broth for each replicate (10 min, 4500 rpm, GS-15R Centrifuge, Beckman Coulter). After the supernatant was decanted, the biomass pellets were immediately placed in aluminum racks at  $-20^{\circ}\text{C}$ .

For biovolume (BV) measurements, cultivation samples were diluted 1:200 or 1:2,000 depending on the biomass concentration in 10 mL CASYton buffer (OMNI Life Science GmbH). The size distribution of the sample was determined by the MultiSizer3 Coulter Counter (Beckman Coulter) and the biovolume was computed by calculating the first moment of the distribution, assuming a spherical shape of the measured cells. Cell dry weight (CDW) was determined by centrifuging 2 mL of a bioreactor

sample in a pre-dried and pre-weighted Eppendorf tube at 13,000 rpm for 7 min. The cells were washed in 1 mL 0.9% (w v $^{-1}$ ) NaCl by resuspension and renewed centrifugation. After decanting the supernatant, the pellets were dried for at least 2 days at  $80^{\circ}\text{C}$ .

A correlation between BV in  $\mu\text{L mL}^{-1}$  and CDW in  $\text{g L}^{-1}$  was derived for the  $\Delta\text{pyc } \Delta\text{odx}$ ,  $\Delta\text{ppc } \Delta\text{malE}$  and WT strain (see **Supplementary Figure 3**) and then applied to calculate the CDW for all cultivations assuming a standard deviation of 5%.

## Estimation of Extracellular Rates

Specific rates for biomass growth ( $\mu$ ) and D-glucose uptake ( $\pi_{\text{GLC}}$ ) were estimated using a model-based approach and process data from the exponential phases of corresponding batch cultivations. In short, the remaining D-glucose concentration  $c_{\text{GLC}}(t)$  at any given time point  $t$  is the integral over the volumetric uptake rate  $\pi_{\text{GLC},\text{vol}}(t)$  given in  $\text{mmol L}^{-1} \text{ h}^{-1}$ :

$$c_{\text{GLC}}(t) = c_{\text{GLC},0} - \int_{t_0}^t \pi_{\text{GLC},\text{vol}}(t') dt \quad (1)$$

Assuming a constant D-glucose uptake from exponentially growing cells, it holds:

$$\pi_{GLC,vol}(t) = \pi_{GLC} \cdot X(t) \quad (2)$$

where  $X(t) = X_0 \cdot e^{\mu \cdot t}$  denotes the biomass concentration in  $\mu\text{L mL}^{-1}$  or  $\text{g L}^{-1}$ , depending on whether the biomass signal is BV or CDW. Inserting Equations (2) into (1) and carrying out the integration yields:

$$c_{GLC}(t) = C - \frac{\pi_{GLC}}{\mu} \cdot X_0 \cdot e^{\mu \cdot t} \quad (3)$$

with model parameters  $X_0$ ,  $\mu$ ,  $\pi_{GLC}$ , and  $C$ , where the latter absorbs the integration constant and the initial substrate concentration. Equations (2) and (3) were jointly fitted to the experimentally observed time courses of biomass and substrate concentration, respectively. The end of the exponential phase was judged by the peak in  $\text{CO}_2$  volume fraction in the exhaust gas stream (see **Supplementary Figure 2**).

The fitting procedure was carried out using a sequential quadratic programming optimization routine from MATLAB (Mathworks Inc., R2019b). The estimation of confidence intervals was based on a parametric Monte Carlo bootstrapping approach from literature (Dalman et al., 2013). In short, every available measurement was perturbed independently within the normal distribution described by the measurement value and its standard deviation of the respective measurement. The perturbation operation consisted in sampling from the normal distribution of each measurement point and inserting the sample as measurements. The above-described variance-weighted least-square fit was then re-performed. The sample was generated as a Latin-Hypercube sample using the `lhs`-function of MATLAB and comprised 1,000 samples if not otherwise stated. The upper and lower confidence bounds were then derived as the  $\alpha$ -th and  $(1-\alpha)$ -th percentile of the parameter sample obtained from 1000 least-squared fits. If not otherwise stated  $\alpha$  is set to 0.25, the confidence interval being the Interquartile Range (IQR).

The total  $\text{CO}_2$  formation rate  $\pi_{CO_2,tot}(t)$  given in  $\text{mol h}^{-1}$  was calculated from balancing the gas phase of the bioreactor as:

$$\pi_{CO_2,tot}(t) = \frac{F \cdot p}{R \cdot T} \left[ \frac{100 - \Phi_{O_2}^\alpha - \Phi_{CO_2}^\alpha}{100 - \Phi_{O_2}^\omega(t) - \Phi_{CO_2}^\omega(t)} \cdot \frac{\Phi_{CO_2}^\omega(t)}{100} - \frac{\Phi_{CO_2}^\alpha}{100} \right] \quad (4)$$

where  $\Phi$  denotes the volume fraction of the gas species in question in vol% and the superscripts  $\alpha$  and  $\omega$  denote the inlet and outlet concentrations, respectively.  $F$  denotes the inlet air flow in  $\text{m}^3 \text{ h}^{-1}$ . The biomass-specific carbon dioxide formation rate  $\pi_{CO_2}(t)$  given in  $\text{mmol g}_{CDW}^{-1} \text{ h}^{-1}$  or  $\text{mmol mL}_{BV}^{-1} \text{ h}^{-1}$ , respectively, was obtained by dividing  $\pi_{CO_2,tot}(t)$  by  $X(t)$  at time point  $t$ .

The complete set of extracellular rate estimates for all independent bioreactor cultivation experiments can be found in **Supplementary Table 1**.

## Quantitative Metabolomics

The metabolome samples of all strains were spiked with identical internal standard and were measured in one acquisition batch on the LC-ESI-QqQ MS system. Organic acids and unstable sugar phosphates were measured within 24 h from the extraction of samples. Quenching, cell separation, cell extraction, isotope dilution mass spectrometry and metabolite leakage correction were performed according to previous protocols (Paczia et al., 2012; Tillack et al., 2012).

For quantification of organic acids, samples were separated using a synergy hydro C18 reversed phase column (Phenomenex) on an Agilent 1200 chromatography system (Agilent Technologies). The HPLC column outlet was coupled to a QqQ MS device (API 4000, AB Sciex) equipped with a TurboSpray ion source in negative ionization mode. The elution was isocratic at 84% buffer A and 16% buffer B at a flowrate of  $0.45 \text{ mL min}^{-1}$  at  $20^\circ\text{C}$ . The eluents were as follows: Buffer A: 10 mM tributylamine, 15 mM acetic acid, pH 4.95; Buffer B: methanol. MS parameters were as follows: CAD (collision gas pressure): 5, CUR (curtain gas flow): 30, GS1 (nebulizer gas flow): 70, GS2 (turbo heater gas flow): 70, IS (electrospray voltage):  $-4,500 \text{ V}$ , TEM (heater gas temperature):  $650^\circ\text{C}$ , entrance potential:  $-10 \text{ eV}$ . Injection volume was  $10 \mu\text{L}$ .

For quantification of amino acids, samples were separated using Luna SCX cation exchange column at  $60^\circ\text{C}$  on a JASCO HPLC system. The following buffers were employed: Buffer A: 5% acetic acid, B: 15 mM ammonium acetate. The applied elution gradient can be found in **Supplementary Table 2**. Injection volume was  $10 \mu\text{L}$ .

For quantification of sugar and nucleoside phosphates, samples were separated on a synergy hydro C18 reversed phase column at  $40^\circ\text{C}$ . Eluent were Buffer A: 10 mM tributylamine, 15 mM acetic acid, pH 4.95 and Buffer B: methanol. The HPLC system, the QqQ MS device and its MS parameter settings were the same as for the LC-MS/MS method for organic acids. For quantification the gradient of **Supplementary Table 3** was applied. Injection volume was  $10 \mu\text{L}$ .

## Generation of Ion Libraries for Proteomics

To populate our *C. glutamicum* ion library, separate IDA acquisitions of samples of *C. glutamicum* WT cultivated as described above but with different carbon sources were performed. In each cultivation the carbon source was either 55 mM D-glucose, 111 mM sodium pyruvate, 83 mM disodium-L-malate, 55 mM sodium citrate or 48 mM sodium benzoate. Each sample was lysed and  $100 \mu\text{g}$  protein thereof digested and processed as described elsewhere (Voges and Noack, 2012).

These samples were separated on a Agilent 1260 Infinity HPLC system (Agilent Technologies) equipped with a  $150 * 2.1 \text{ mm Ascentis Express Peptide ES-C18}$  column with  $2.7 \mu\text{m}$  particle size and an appropriate  $5 * 0.3 \text{ mm Acclaim PepMap Trap Cartridge}$  (Thermo Scientific) which were both maintained at  $25^\circ\text{C}$  and a flow rate of  $200 \mu\text{L min}^{-1}$ . For LC separation 0.1% formic acid in LC-MS grade water ( $\text{v v}^{-1}$ ) was used as buffer A, whereas buffer B was 0.1% formic acid in LC-MS grade acetonitrile ( $\text{v v}^{-1}$ ). Before each injection, the column was equilibrated for 12 min at 97% A. After  $20 \mu\text{L}$  were injected, the

gradient of **Supplementary Table 4** was applied. The LC-eluent was coupled to an ESI-QqTOF MS (TripleTOF 6600, AB Sciex) equipped with an DuoSpray ion source. The data acquisition was performed using Analyst TF 1.8 (AB Sciex). An information-dependent acquisition was performed on each injection during which all ions with  $m/z > 300$ , charge state 2–4 and above intensity of 150 were selected for fragmentation.

The acquired MS<sub>2</sub> spectra of the *C. glutamicum* digests were searched against a FASTA database of *C. glutamicum* ATCC 13032 (GenBank assembly accession: GCA\_000196335.1) using ProteinPilot software 5.0 (AB Sciex) employing default probabilities for biological modifications. The confidently identified peptides of each injection were assembled into a library covering 1727 ORFs. This library incorporates the peptide confidence after identification, peptide (precursor) intensity in the MS<sub>1</sub> scan from the IDA acquisition, fragment ion intensities and the observed peptide retention time.

### SWATH Acquisition

Starting from an IDA acquisition of each organism variable SWATH windows were calculated using the SWATH Variable Window Calculator 1.0 (AB Sciex). Using these windows, a SWATH acquisition method was set up, which employed the same chromatographic gradient and ion source setting as the IDA acquisition. The window width and CE ramp parameters can be found in **Supplementary Table 5**. For SWATH acquisition a digest of each sample was prepared according to the protocol of Voges and Noack, which involves mixing 50 µg unlabeled sample protein and 50 µg internal standard from a separate cultivation of *C. glutamicum* with  $(^{15}\text{NH}_4)_2\text{SO}_4$  (Voges and Noack, 2012). Ten microliter of each sample was injected.

### SWATH MS Data Processing

SWATH data processing was performed using the MS/MS<sup>all</sup> SWATH Acquisition MicroApp in PeakView 2.2 (AB Sciex). The ion library from above was imported from ProteinPilot into this app by excluding shared peptides but not modified ones. From the imported ion library the ten most intense peptides were selected for quantification provided they had a peptide confidence of >96%. The intensity selection is based on the MS<sub>1</sub> survey scan intensity of each peptide in the IDA runs used to build the ion library. If <10 peptides fulfilled the above criterion for a protein, only the available peptides were quantified.

For each peptide group the 12 most intense fragment ion traces were chosen by the SWATH processing algorithm. This algorithm favors the most intense fragment ion traces from the library spectrum whose  $m/z$  value lies above the Q1 window of their precursor ion. For each fragment ion, within 5 min around the expected retention time, an unlabeled mass trace was extracted from the SWATH spectra within  $\pm 15$  ppm of its monoisotopic mass, whereas the labeled mass trace was extracted within  $\pm 15$  ppm of its fully  $^{15}\text{N}$ -labeled isotopologue. All transitions of one peptide were assembled into a so called peak group which was scored for congruency with the ion library. The false discovery rate was set to 0.1%. The finished processing session was saved as MarkerView file (.mrkvw extension), which was opened in MarkerView 1.3.1 (AB Sciex) for estimation of

fold-changes (ratio of means) of protein levels between mutant and control.

### Elemental Analysis of Biomass

The concentration of carbon, nitrogen and sulfur in biomass were determined at the central Analytical core facility of Forschungszentrum Jülich (ZEA-3). Biomass samples from the early stationary phase were processed following the same procedure as for CDW content determination. The dried biomass pellet was ground to a fine powder in a pre-dried mortar using a pre-dried pestle and sent in a sealed container to ZEA-3.

## RESULTS AND DISCUSSION

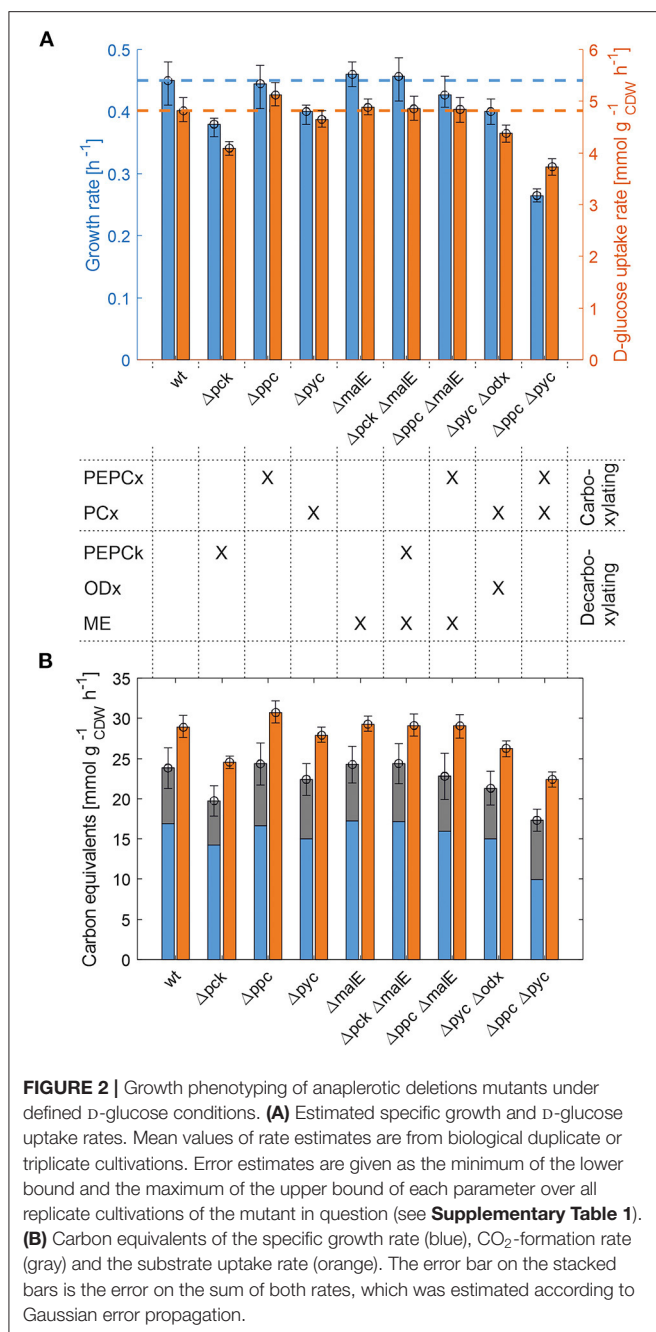
### Growth Phenotyping of Anaplerotic Deletions Mutants Under Defined D-Glucose Conditions

In our previous flux identifiability analysis focusing on the anaplerotic node in *C. glutamicum* those metabolic network structures were identified that are structurally identifiable under defined D-glucose conditions (Kappelmann et al., 2016). These structures are based on deletions of specific genes encoding for anaplerotic reactions. In this study, we comprehensively analyzed a set of mutant strains for which a unique solution using  $^{13}\text{C}$ -MFA theoretically exists as well as mutants that are non-flux-identifiable strains.

All selected deletion mutants were able to grow on defined CGXII medium with D-glucose as sole carbon and energy source, except for strain *C. glutamicum*  $\Delta ppc \Delta pyc$  that is deficient in PEPCx and PCx activity (**Table 1**). While this mutant was able to grow on acetate without lag-phase no biomass formation could be monitored within 48 h cultivation on D-glucose and this observation is concordant with Peters-Wendisch et al. (1998). However, prolonged incubation of *C. glutamicum*  $\Delta ppc \Delta pyc$  under defined D-glucose conditions in a microbioreactor setup and at different inoculum sizes always resulted in the onset of growth after 75 h or later, mainly after 100 h (**Supplementary Figure 1**).

The whole mutant library was then cultivated under controlled bioreactor conditions on defined CGXII medium with 1% D-glucose. Specific growth and substrate uptake rates were estimated using a model-based approach (see Materials and Methods section). The D-glucose uptake rate of  $4.82 \text{ mmol g}_{\text{CDW}}^{-1} \text{ h}^{-1}$  and the specific growth rate of  $0.45 \text{ h}^{-1}$  for *C. glutamicum* WT agree well with literature (Buchholz et al., 2014). Based on the determined confidence intervals discernible growth phenotypes can be identified among the set of deletion mutants (**Figure 2A** and **Table 2**).

First, the *C. glutamicum*  $\Delta pck$  mutant showed a lower growth rate although PEPCk catalyzes a gluconeogenetic reaction, not needed under glycolytic conditions to supply biomass precursors. However, the observed growth defect clearly indicates its activity under glycolytic conditions. This result was also obtained in the study of Riedel et al. with the comparable genotype (**Table 2**) and in the study of Petersen et al. (2001), who inferred PEPCk activity in a *C. glutamicum* L-lysine producer from  $^{13}\text{C}$ -labeling data.



Since the carbon flow catalyzed by PEPCk is of opposite direction compared to the overall carbon flow under glycolytic conditions, its catalytic effect must be of indirect nature. Strangely, the double deletion mutant *C. glutamicum* Δpck ΔmalE showed a restored growth phenotype, with a growth rate equivalent to the WT.

Deletion mutants comprising a deletion in PEPCx do not show a significantly altered growth phenotype as long as PCx is still active (**Figure 2A** and **Table 2**). The stoichiometry of the reaction catalyzed by PEPCx is identical to the reaction sequence of pyruvate kinase (PK) and PCx, which apparently fully compensates for the missing carboxylation activity of

PEPCx. On the other hand, mutant strains *C. glutamicum* Δpyc and *C. glutamicum* Δpyc Δodx do exhibit a growth phenotype. This finding underscores the role of PCx as most important anaplerotic reaction under aerobic conditions and suggests that its catalyzed flux is most likely greater than that of PEPCx in the WT under standard D-glucose conditions. Noteworthy, a *C. glutamicum* mutant with single deletion of the *odx* gene was shown to grow equally well as the wild type (Klaffl and Eikmanns, 2010).

The evolved *C. glutamicum* Δppc Δpyc strain, missing both carboxylation activities shows a greatly reduced growth rate of 0.27 h<sup>-1</sup> (**Figure 2A** and **Table 2**). In the absence of both PEPCx and PCx, three other and different anaplerotic activities can possibly substitute the anaplerotic activity of PEPCx and PCx: First, ME may catalyze the carboxylation of pyruvate to malate in an NADPH-dependent manner. This appears plausible since ME was found to catalyze this reaction sequence in *in vitro* assays (Cocaign-Bousquet et al., 1996; Gourdon et al., 2000). Moreover, it could be experimentally shown that a NADPH-dependent ME from *E. coli* can act as sole anaplerotic enzyme in *Saccharomyces cerevisiae* sustaining a growth rate of 0.06 h<sup>-1</sup> (Zelle et al., 2011). Second, PEPCk may act in reverse direction from phosphoenolpyruvate to oxaloacetate. This hypothesis is rather unlikely as this reaction directionality would couple anaplerotic carboxylation to the substrate level phosphorylation, generating one GTP molecule. Since the reaction from oxaloacetate to phosphoenolpyruvate is coupled to the hydrolysis of one GTP molecule, it can be expected to be favored. A third alternative represents the glyoxylate shunt, which exclusively fulfills the anaplerotic function in *C. glutamicum* under growth on acetate (Wendisch et al., 1997).

## A Closer Look Into Carbon Balancing

Interestingly, the *C. glutamicum* Δppc Δpyc mutant also showed an altered ratio of specific glucose uptake and growth rate in comparison to other mutants and the WT (**Figure 2A**). The observation that less biomass was formed per unit uptake rate raised the question as to where the excess carbon atoms end up. To answer this question, a carbon balance was performed. Contrary to the conventional carbon balancing approach, consisting in the quantification of the total carbon recovery in biomass and exhaust gas by the time all substrate has been consumed (Buchholz et al., 2014), we calculated the instantaneous carbon balance Θ as:

$$\Theta = \frac{\mu \cdot \omega_C}{M_C} + \pi_{CO_2} - \pi_{GLC} \cdot 6 \quad (5)$$

where  $\mu$  denotes the specific growth rate given in h<sup>-1</sup> (here assumed to be constant for the considered exponentially growing cells),  $\omega_C$  denotes the mass fraction of carbon in the biomass in g<sub>CDW</sub><sup>-1</sup>,  $M_C$  denotes the molecular weight of carbon in g mmol<sup>-1</sup>, and  $\pi_{GLC}$  as well as  $\pi_{CO_2}$  denote the specific D-glucose uptake and carbon dioxide formation rates as derived from Equations (2) to (4).

Equation (5) balances the specific rates of carbon uptake and carbon flow into sinks at any given time. Here biomass and

**TABLE 2 |** Estimated specific growth rates ( $\mu$ ), D-glucose consumption rates ( $\pi_{\text{GLC}}$ ), CO<sub>2</sub> formation rates ( $\pi_{\text{CO}_2}$ ), and instantaneous carbon balance ( $\theta$ ) for anaplerotic deletion mutants during exponential growth.

Strain	$\mu$ [h <sup>-1</sup> ]	$\pi_{\text{GLC}}$ [mmol g <sup>-1</sup> CDW h <sup>-1</sup> ]	$\pi_{\text{CO}_2}$ [mmol g <sup>-1</sup> CDW h <sup>-1</sup> ]	$\theta$ [-]	Conditions	References
<i>C. glutamicum</i> ATCC 13032	0.44	–	–	–	Shake flask	Riedel et al., 2001
	0.40 <sup>a</sup>	–	–	–	Bioreactor	Blombach et al., 2013
	0.45 ± 0.04	4.82 ± 0.25	6.94 ± 0.71	0.82 ± 0.089	Bioreactor	This work
<i>C. glutamicum</i> Δ <pck< p=""></pck<>	0.40	–	–	–	Shake flask	Riedel et al., 2001
	0.30 <sup>a</sup>	–	–	–	Bioreactor	Blombach et al., 2013
	0.38 ± 0.02	4.10 ± 0.14	5.51 ± 0.53	0.81 ± 0.077	Bioreactor	This work
<i>C. glutamicum</i> Δ <pcc< p=""></pcc<>	Equal to WT	–	–	–	Shake flask	Peters-Wendisch et al., 1993, 1996
	0.34 <sup>a</sup>	–	–	–	Bioreactor	Blombach et al., 2013
	0.45 ± 0.04	5.12 ± 0.24	7.64 ± 1.09	0.79 ± 0.083	Bioreactor	This work
<i>C. glutamicum</i> Δ <pyc< p=""></pyc<>	Nearly WT	–	–	–	Shake flask	Peters-Wendisch et al., 1998
	0.30 <sup>a</sup>	–	–	–	Bioreactor	Blombach et al., 2013
	0.40 ± 0.02	4.65 ± 0.17	7.43 ± 0.76	0.80 ± 0.072	Bioreactor	This work
<i>C. glutamicum</i> ΔmalE	Equal to WT	–	–	–	Shake flask	Gourdon et al., 2000
	0.34 <sup>a</sup>	–	–	–	Bioreactor	Blombach et al., 2013
	0.46 ± 0.02	4.88 ± 0.17	7.00 ± 1.00	0.84 ± 0.080	Bioreactor	This work
<i>C. glutamicum</i> Δ <pck< p=""> ΔmalE</pck<>	0.46 ± 0.04	4.85 ± 0.24	7.27 ± 0.83	0.83 ± 0.087	Bioreactor	This work
<i>C. glutamicum</i> Δ <pcc< i=""> ΔmalE</pcc<>	0.43 ± 0.03	4.84 ± 0.25	6.79 ± 1.92	0.79 ± 0.088	Bioreactor	This work
<i>C. glutamicum</i> Δpyc Δodx	0.40 ± 0.02	4.38 ± 0.17	6.31 ± 0.99	0.81 ± 0.078	Bioreactor	This work
<i>C. glutamicum</i> Δ <pcc< i=""> Δpyc<sup>b</sup></pcc<>	No growth	–	–	–	Shake flask	Peters-Wendisch et al., 1998
	0.27 ± 0.01	3.74 ± 0.16	7.40 ± 0.68	0.78 ± 0.070	Bioreactor	This work

Comparison of own data with available literature data for cultivation experiments with the specified strains on defined CGXII media and D-glucose as sole carbon and energy source. Data from *C. glutamicum* ATCC 13032 (WT) was only included from studies with corresponding deletion mutants. In case no quantitative data was available a qualitative comparison was made.

<sup>a</sup>Aeration was limited to 0.1 vvm and the media contained no initial protocatechic acid.

<sup>b</sup>Evolved strain after prolonged cultivation in CGXII media with D-glucose as sole carbon and energy source.

CO<sub>2</sub> formation are the only considered carbon sinks (any other by-product formation could be excluded for all strains under investigation). The quantity  $\omega_C$  has been reported several times in the literature: Marx et al. (1996) reported 0.408 gC g<sup>-1</sup> CDW for *C. glutamicum* MH20-22B, a L-lysine producer strain, determined in freeze-dried biomass with a CHNS elemental analyzer. More recently, Buchholz et al. (2014) reported a value of 0.514 gC g<sup>-1</sup> CDW for *C. glutamicum* ATCC 13032, which was determined by separately quantifying the total carbon in liquid bioreactor samples (supernatant and biomass) and the total inorganic carbon (total dissolved carbon) in the supernatant. In this work, we experimentally quantified  $\omega_C$  for wild-type *C. glutamicum* to be around 0.4–0.42 gC g<sup>-1</sup> CDW. The uncertainty of this parameter notwithstanding, its value was assumed to be 0.45 gC g<sup>-1</sup> CDW for all following calculations. In face of the apparent uncertainty, its standard error was assumed to be 0.05 gC g<sup>-1</sup> CDW. The arising interval covers all available literature information on this quantity. The uncertainty

in derived quantities thereof can be computed by Gaussian error propagation.

From **Figure 2B** it becomes apparent that the evolved Δ Δpyc strain grows with a higher relative CO<sub>2</sub>-formation rate with respect to the uptake rate. At the same time, the sum of the specific rates at which carbon flows into sinks amounts to the same relative value with respect to the carbon uptake rate as in other strains. Therefore, it seems plausible that a higher decarboxylation activity explains the lower relative growth rate in the *C. glutamicum* Δ Δpyc mutant. This higher relative CO<sub>2</sub>-formation rate further substantiates the hypothesis that an altered ratio of ICL and ICD activity involves the glyoxylate shunt as anaplerotic reaction sequence in this mutant. Exclusive anaplerotic activity through the glyoxylate shunt would release two equivalents CO<sub>2</sub> per C4-body of oxaloacetate formed, instead of fixing one CO<sub>2</sub> as in the case of alternative ME or reversible PEPCK activities.

One result holds true irrespective of the genetic background: The recovery of carbon at any given time in the reactions that act as carbon sinks amounts to 80% of the carbon equivalent of the uptake rate (**Figure 2B** and **Table 2**). The non-closed instantaneous carbon balance may hint to extensive by-product formation or indicate systematically biased extracellular rates. The former is unlikely since *C. glutamicum* WT is known to produce only minor by-products under aerobic conditions (the DO was maintained at 30%). Notwithstanding, the genetic alterations may induce a more extensive overflow metabolism in some deletion mutants. However, all organic acids, sugar phosphates and amino acids in the culture supernatant measured by targeted LC-MS/MS account for a total of  $274\text{--}786 \mu\text{mol C g}_{\text{CDW}}^{-1}$ , depending on the strain. Therefore, the exometabolome can be neglected as carbon sink since the gap in the balance of specific rates amounts to several  $\text{mmol}_C \text{g}_{\text{CDW}}^{-1} \text{ h}^{-1}$  (**Figure 2B**).

Remarkably, the value of 80% for the instantaneous carbon balance matches the determined carbon balance closure in the study of Buchholz et al. (2014). This study convincingly showed that the gap in carbon balance can be traced back to the fact that part of the  $\text{CO}_2$ -production at any given time dissolves as  $\text{HCO}_3^-$  in the culture broth. This share is not recovered as gaseous  $\text{CO}_2$  at the detector, leading to an underestimation of the  $\text{CO}_2$ -production rate.

## Proteomic and Metabolomic Responses to Gene Deletions in Anaplerotic Reactions

To gain further insight into the metabolism of each mutant, untargeted proteome and targeted metabolome analyses were performed. To ensure comparability, eight strains were cultivated in parallel and subjected to identical and isochronous sample processing in subsequent steps (see section Materials and Methods for detailed descriptions). In total, we analyzed 1199 cytosolic proteins and 48 metabolites of central metabolism.

Since the  $\Delta ppc$  mutant showed no altered phenotype and has been thoroughly characterized before, it was omitted from the set of strains to be analyzed. The evolved strain *C. glutamicum*  $\Delta ppc$   $\Delta pyc$  showed significant changes in specific proteins and metabolites, which will be discussed separately in the next section.

Further differentially expressed proteins were found in *C. glutamicum*  $\Delta pck$  and *C. glutamicum*  $\Delta pyc$  (**Figure 3**). In none of the other tested deletion mutants significantly changed protein abundances [ $p < 0.05$ ,  $|\text{Log2(fold change)}| \geq 0.5$ ] were found (data not shown).

Only one protein encoded by *cypD* (cg0282) and which might be involved in stress response was found to be up-regulated in the *C. glutamicum*  $\Delta pck$  mutant (**Table 3**). In *C. glutamicum*  $\Delta pyc$  the enzyme quinolinate synthase A encoded by the *nadA* gene (cg1216) was up-regulated. This enzyme catalyzes the condensation of iminoaspartate with dihydroxyacetone phosphate to form quinolinate, and represents the second step of the *de novo* synthesis of  $\text{NAD}^+$ . The latter starts from L-aspartate and up-regulation of this enzyme could be a cellular response to the limited availability of this amino acid following the inactivation of PCx and to ensure sufficient  $\text{NAD}^+$  supply. In

addition, the putative transcriptional regulator (cg0787) and the 50S ribosomal protein L36 encoded by the *rpmJ* gene (cg2791) were found to be down-regulated in *C. glutamicum*  $\Delta pyc$ .

**Figure 4** shows intracellular and extracellular concentrations of selected metabolites. The L-aspartate pool is most closely correlated with the growth rate, i.e., the lowest concentrations were observed for all mutants with reduced growth rate. Apparently, its supply appears to be limiting the growth as the restored growth rate of the  $\Delta pck$   $\Delta malE$  mutant in comparison to the single deletion strain  $\Delta pck$  goes hand in hand with increased L-aspartate supply. The concentration pattern of L-aspartate seems to reflect itself in the L-homoserine pool, which is derived from the former through three intermediate reaction steps, consuming two  $\text{NAD(P)H}$  molecules and one ATP molecule. In contradistinction to L-aspartate, however, L-homoserine is clearly higher concentrated in the  $\Delta pck$  mutant. Since the reaction sequence between both intermediates is redox-dependent, one may be tempted to attribute this observation to redox balancing. The biosynthesis of L-glutamate from  $\alpha$ -ketoglutarate and of L-proline from L-glutamate are also redox-dependent. Conspicuously, both pools are also higher concentrated in this strain (**Figure 4**).

Moreover, we analyzed intracellular levels of NADPH and NADH alongside their oxidized analogs. No significant difference was detected in the reduced forms of these co-factors (data not shown). However, the mean of relative standard deviation over all mutants for NADH and NADPH concentrations amounts to 46% and 48%, respectively. This high technical error, impeding a precise quantification, cannot be traced back to inaccuracies in pipetting or BV concentration measurements since these factors also apply to all other metabolite quantifications in the same sample. Since the mean relative standard deviation for other metabolite pools was below 10% these factors appear to have been controlled quite well. The most likely reason for the observed coefficients of variation is metabolite instability. The redox equivalents are known to be quite sensitive to oxidation and degradation (Siegel et al., 2014). Slightly different temperature time courses, residual enzymatic activity in metabolite extracts and oxidation most likely account for the observed differences. Therefore, no accurate conclusion about the redox state in each mutant could be drawn. Nonetheless, the fact that the removal of a redox-dependent enzyme like ME restores the growth rate of the *C. glutamicum*  $\Delta pck$  mutant suggests an involvement of the redox balance mediating some of the observed changes in metabolite pools.

## Glyoxylate Shunt Enables Growth of *C. glutamicum* $\Delta ppc$ $\Delta pyc$ on D-Glucose as Sole Carbon and Energy Source

Whole-genome sequencing of evolved *C. glutamicum*  $\Delta ppc$   $\Delta pyc$  confirmed the absence of genes *ppc* and *pyc* across the cell population (**Table 4**), excluding any growth contamination effect. Two insertions and some SNPs (see **Supplementary Table 6**) were detected in the coding region for ICD. Moreover, ICL (cg2560), MS (cg2559), and *cis*-aconitase (ACN, cg1737) are highly up-regulated in *C. glutamicum*  $\Delta ppc$   $\Delta pyc$  (**Figure 3** and

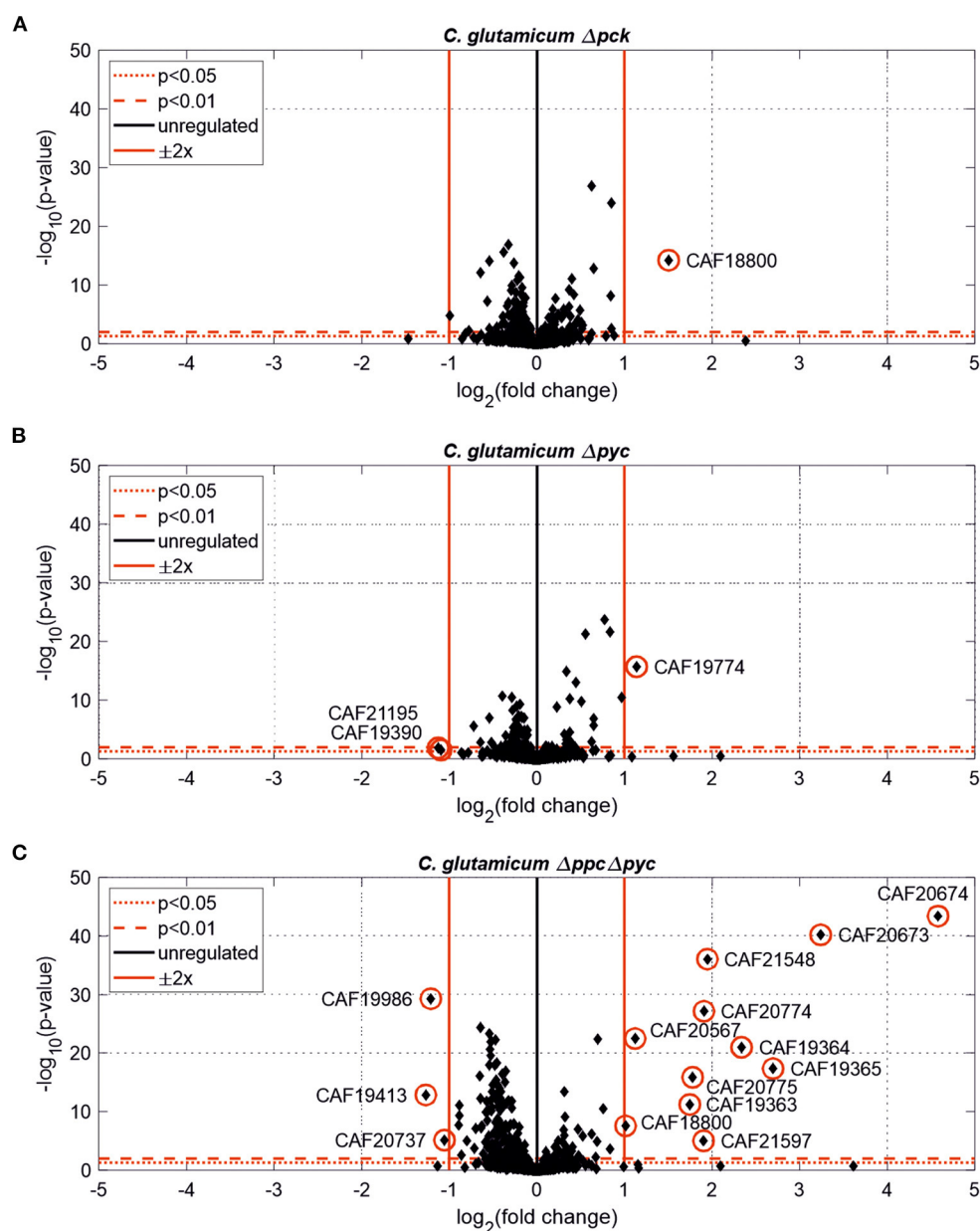


**FIGURE 3 |** Estimated protein fold-changes for selected *C. glutamicum* deletion mutants in comparison to the wild type. **(A)** *C. glutamicum*  $\Delta pck$ . **(B)** *C. glutamicum*  $\Delta pyc$ . **(C)** *C. glutamicum*  $\Delta ppc \Delta pyc$ . Volcano plots with significantly changed proteins [ $p < 0.05$ ,  $|\log_2(\text{fold change})| \geq 0.5$ ] highlighted in red.

**Table 3**) and only in this mutant intracellular and extracellular accumulation of glyoxylate was detected (**Figure 4**).

These findings are in agreement with the study of Schwentner et al. and point to a redirection of carbon flux in our evolved strain from the oxidative decarboxylation branch of the TCA cycle into the glyoxylate shunt (Schwentner et al., 2018). In the absence of C3-carboxylation activity at the anaplerotic node, accumulation of the substrate pools phosphoenolpyruvate and pyruvate can be expected. Indeed, phosphoenolpyruvate was significantly higher concentrated in the evolved  $\Delta ppc \Delta pyc$

strain, while the intracellular pyruvate pool remained unaffected (**Figure 4**). However, metabolite levels of L-alanine and L-valine, which are directly derived from pyruvate, were strongly increased and this finding is also consistent with previous data (Schwentner et al., 2018). The lack of statistical significance of strain differences in the pyruvate pool is most likely due to higher technical errors during metabolite quantification. It is well-established that the accurate quantification of organic acids in cell extracts represents a veritable challenge (Zimmermann et al., 2014).

**TABLE 3 |** Differentially expressed proteins of *C. glutamicum* anaplerotic deletion mutants in comparison to the wild-type strain.

Strain	Protein ID	Cg no.	Gene	Annotated function	Fold change	p-value
<i>C. glutamicum</i> Δpck	CAF18800	cg0282	cybD	Putative protein, CsbD-family, probably involved in stress response	2.84	5.90e-15
<i>C. glutamicum</i> Δpyc	CAF19774	cg1216	nadA	Quinolinate synthase A	2.20	2.03e-16
	CAF19390	cg0787	–	Transcriptional regulator	0.47	3.11e-02
	CAF21195	cg2791	rpmJ	50S ribosomal protein L36	0.46	1.40e-02
<i>C. glutamicum</i> Δppc Δpyc	CAF20674	cg2560	aceA	Isocitrate lyase	23.94	3.79e-44
	CAF20673	cg2559	aceB	Malate synthase	9.45	6.63e-41
	CAF19365	cg0762	prpC2	2-methylcitrate synthase	6.49	4.73e-18
	CAF19364	cg0760	prpB2	2-methylcitrate lyase	5.05	1.07e-21
	CAF21548	cg1737	acn	Aconitase	3.86	8.53e-37
	CAF20774	cg3047	ackA	Acetate kinase	3.75	7.39e-28
	CAF21597	cg1792	whiA	Putative transcriptional regulator-WhiA homolog	3.75	9.38e-06
	CAF20775	cg3048	pta	Phosphate acetyltransferase	3.43	1.42e-16
	CAF19363	cg0759	prpD2	2-methylcitrate dehydratase	3.36	5.83e-12
	CAF20567	–	–	Hypothetical protein	2.18	3.42e-23
	CAF18800	cg0282	–	Conserved hypothetical protein	2.02	2.79e-08
	CAF20737	cg3008	porA	Porin	0.48	7.16e-06
	CAF19986	cg1451	serA	Phosphoglycerate dehydrogenase	0.43	5.03e-30
	CAF19413	cg0812	dtsR1	Acetyl/ propionyl-CoA carboxylase beta chain	0.42	1.34e-13

All proteins with significant changes [ $p < 0.05$ ,  $\text{Log}_2(\text{fold change}) > 0.5$  for upregulated proteins and  $\text{Log}_2(\text{fold change}) < -0.5$  for down-regulated proteins] are listed.

Moreover, the metabolite pool of L-glycine shows one of the most significant concentration changes, clearly distinguishing the evolved Δppc Δpyc strain. L-glycine, in turn, is derived from L-serine, which also showed an increased concentration (**Figure 4**). It appears that the missing carboxylation rate cannot be matched by the pyruvate dehydrogenase activity in the Δppc Δpyc mutant for substrate pools like phosphoenolpyruvate as well as amino acids derived from the lower glycolytic intermediates appear to accumulate intracellularly. This would also explain why the phosphoglycerate dehydrogenase encoded by serA (cg1451) was found to be significantly down-regulated in this mutant (**Table 3**). The enzyme catalyzes the first step in the biosynthesis of L-glycine, L-serine and L-cysteine and its down-regulation could be the cellular response to the higher availability of 3-phosphoglycerate.

In terms of glyoxylate shunt regulation, Wendisch et al. suggested that the carbon-source dependent regulation of this pathway is mediated by intracellular acetyl-CoA concentrations (Wendisch et al., 1997). However, intracellular acetyl-CoA concentrations did not vary significantly with respect to strain background (**Figure 4**), and therefore this hypothesis could not be validated with the made intracellular measurements. Unfortunately, acetyl-CoA measurements are notoriously error-prone due to the high instability of thioesters. Though taking strenuous efforts to keep the sample below –20°C and immediate analysis after extraction, we still obtained a highly variable signal within each treatment group.

The corresponding genes aceA and aceB of ICL and MS, respectively, are thought to be repressed by the regulator protein RamB (cg0444) under glycolytic conditions (Auchter et al., 2011). Moreover, it has been established that RamA (cg2831) acts as transcriptional activator of both genes when acetate is the carbon

source. However, no significant change in the abundances of RamA and RamB were found in Δppc Δpyc mutant compared to the wild type. The fact that a ΔramA mutant is not able to grow on acetate suggests that RamA is strictly required as transcriptional activator for increased expression of at least one of the essential enzymes of acetate assimilation, which are acetate kinase (AK) encoded by ackA (cg3047), phosphotransacetylase (PTA) encoded by pta (cg3048), ICL and MS (Cramer and Eikmanns, 2007). Indeed, AK and PTA are also significantly up-regulated in the Δppc Δpyc mutant (**Table 3**).

Most interestingly, this strain also shows an up-regulation of the three enzymes of the methylcitrate cycle in *C. glutamicum* (Claes et al., 2002), namely 2-methylcitrate synthase (PrpC2) encoded by prpC2 (cg0762), 2-methylcitrate dehydratase (PrpD2) encoded by prpD2 (cg0759) and 2-methylcitrate lyase (PrpB2) encoded by prpB2 (cg0760) (**Table 3**). Together with the activities of AK and PTA this cycle is known to be the predominant route for the degradation of propionate into pyruvate and succinate (**Figure 1**). In the presence of propionate all three genes are transcriptionally activated by the regulator PrpR (Plassmeier et al., 2012). Under the applied D-glucose conditions, however, no change in the PrpR abundance was detected. Moreover, it was found that the prpDBC2 operon is transcriptionally activated by RamA, but not affected by RamB (Auchter et al., 2011). This makes the conclusion compelling that the concentration of at least one, still unknown, metabolite effector binding to RamA was altered, leading to the activation of the aforementioned genes. Following the strong up-regulation of the prpDBC2 cluster in combination with the glyoxylate shunt it might be speculated that the surplus of pyruvate (from PEPCx and PCx inactivation) and succinate (from ICL activity) is channeled into the methylcitrate cycle,

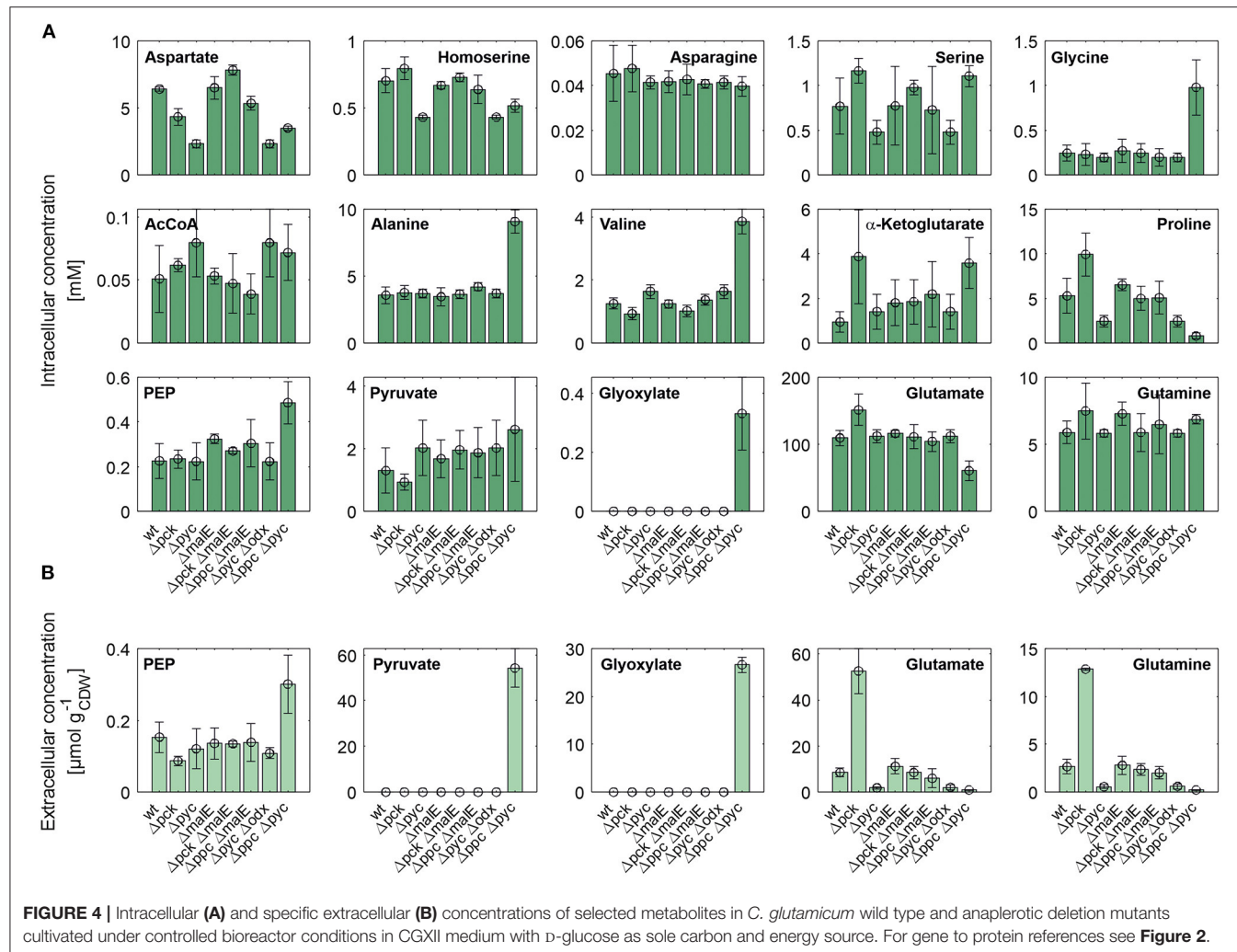


**FIGURE 4 |** Intracellular (**A**) and specific extracellular (**B**) concentrations of selected metabolites in *C. glutamicum* wild type and anaplerotic deletion mutants cultivated under controlled bioreactor conditions in CGXII medium with D-glucose as sole carbon and energy source. For gene to protein references see **Figure 2**.

operating in the reverse direction. This route would represent a by-pass of the TCA cycle reactions succinate: quinone oxidoreductase (SQO), fumarase (FUM) and malate: quinone oxidoreductase (MQO) to provide oxaloacetate as biomass precursor (**Figure 1**). From a thermodynamic point of view, the PrpB2 reaction in direction of 2-methylisocitrate is favored ( $\Delta_r G^{\circ} = -9.3 \text{ kJ/mol}$ ) in comparison to the SQO reaction leading to fumarate ( $\Delta_r G^{\circ} = 14.5 \text{ kJ/mol}$ ). However, the potentially last step of the methylcitrate cycle catalyzed by PrpC2 is thermodynamically very unfavorable ( $\Delta_r G^{\circ} = 39.2 \text{ kJ/mol}$ ), but might still work under *in vivo* conditions due to very low concentrations of oxaloacetate (<100 nM of lower detection limit of applied LC-QQQ MS). Indeed, Plassmeier et al. showed that the *prpDBC2* operon is also expressed under normal cell growth conditions in wild-type *C. glutamicum*, independent of the application of propionate as carbon source (Plassmeier et al., 2007). Moreover, a high up-regulation of the *prpDBC2* operon was found in a *C. glutamicum* strain engineered for overproduction of L-isoleucine (Ma et al., 2018). Here it was speculated that this up-regulation was due to a high intracellular formation of propionyl-CoA, which was derived from the

intermediate 2-ketobutyrate of the L-isoleucine biosynthesis. The resulting propionyl-CoA was then further converted into a polyhydroxyalcanoate by heterologous expression of the *phaCAB* gene cluster. In our case, however, we can exclude propionyl-CoA formation from 2-ketobutyrate because L-aspartate is limiting. Additionally, it remains open what happens with propionyl-CoA as the second product of the PrpC2 reaction when running in reverse direction (**Figure 1**). Therefore, further investigations on the interplay between the different pathways are required to substantiate our hypothesis.

Moreover, we found a SNP in the intergenic region between *cg3314* and *cg3315*, four nucleotides upstream from the translation start of MalR (*malR*, *cg3315*). This protein has been originally identified as repressor of the *malE* gene in the study of Krause et al. (2012) and was recently reported to bind to several other loci (Hünnefeld et al., 2019). Since the mutation occurred outside the coding sequence of this regulator, only expression changes of the gene are able to affect metabolism. Unfortunately, the specific protein data for MalR was not very accurate ( $p > 0.5$ ) to enable any conclusion, but ME appeared to be down-regulated in the evolved  $\Delta ppc \Delta pyc$  strain when grown on D-glucose

**TABLE 4 |** Structural variants identified in the *C. glutamicum*  $\Delta$ *ppc*  $\Delta$ *pyc* mutant adapted to D-glucose as sole carbon source in comparison to *C. glutamicum* WT as reference.

Affected region	Character	nt Region	Length	Reads of position	Rel. frequency
In cg2353, putative protein	Deletion	2,236,684..2,238,317	1,634	47	1
In cg2854, <i>tnp2c</i> , transposase	Deletion	2,716,280..2,717,915	1,636	59	1
In cg0691, <i>groEL'</i> , 60 kDa chaperonin, N-terminal fragment	Deletion	610,994..612,446	1,453	85	0.99
In cg0791, <i>pyc</i> , pyruvate carboxylase	Deletion	707,185..709,613	2,429	76	0.99
In cg1787, <i>ppc</i> , phosphoenolpyruvate carboxylase	Deletion	1,679,298..1,681,219	1,922	60	0.98
Intergenic region of cg1860 (putative membrane protein) and cg1861 ( <i>rel</i> , ppGpp synthetase / ppGpp pyro-phosphorylase)	Replacement	1,754,002..1,754,038	37	73	0.98
Upstream of cg0756, <i>cstA</i> , carbon starvation protein A	Deletion	669,585..669,597	13	46	0.9
In cg2262, <i>ftsY</i> , signal recognition particle GTPase	Deletion	2,144,947..2,144,964	18	13	0.4
In cg0766, <i>icd</i> , isocitrate dehydrogenase	Insertion	681,078..681,079	57	27	0.38
In cg0766, <i>icd</i> , isocitrate dehydrogenase	Insertion	681,136..681,137	57	26	0.32
In cg0953, <i>mctC</i> , monocarboxylic acid transporter	Deletion	884,479..884,487	9	13	0.31

The column "Reads of position" refers to the number of sequencing reads supporting the alteration. The relative frequency refers to the number of reads supporting the alteration relative to the total number of reads of this position or region.

as sole carbon and energy source (0.54-fold,  $p < 4.73e-10$ ). Since purified ME of *C. glutamicum* was shown to carboxylate pyruvate in *in vitro* assays with an apparent  $K_m$  constant of 13.8 mM (Gourdon et al., 2000) it was speculated that ME serves as anaplerotic enzyme under circumstances when PEPCx and PCx activities are absent and pyruvate availability is still ensured through running glycolysis. In our case, however, the amount of ME was significantly reduced with respect to the wild type and its intracellular substrate pool of pyruvate is not significantly altered and well below the  $K_m$  value (Figure 4A). Therefore, it can be excluded that ME catalyzes a flux compensating for the missing PCx and PEPCx activity in the evolved  $\Delta$ *ppc*  $\Delta$ *pyc* strain.

Finally, a deletion was detected in the *mctC* gene (cg0953), which has been shown to be essential in *C. glutamicum* for the uptake of pyruvate (Jolkver et al., 2009). Based on this, it can be hypothesized that the genetic alteration in this transporter may lead to a decreased uptake of pyruvate from the medium, which would explain the extracellular accumulation of pyruvate exclusively found in the  $\Delta$ *ppc*  $\Delta$ *pyc* mutant (Figure 4B).

## CONCLUSIONS

We characterized eight different mutant strains of *C. glutamicum* carrying single or double deletions in five anaplerotic enzymes. The metabolism and adaptation of each mutant during growth

under defined D-glucose conditions in lab-scale bioreactors was investigated by quantification of its extracellular rates, central metabolic intermediates by LC-QqQ MS and proteome by SWATH acquisition using a LC-QqTOF MS platform.

In comparison to the wild type the four deletion mutants *C. glutamicum*  $\Delta$ *pyc*, *C. glutamicum*  $\Delta$ *pyc*  $\Delta$ *odx*, *C. glutamicum*  $\Delta$ *ppc*  $\Delta$ *pyc*, and *C. glutamicum*  $\Delta$ *pck* showed lowered specific growth rates and D-glucose uptake rates, underlining the importance of PCx and PEPCx activity for a balanced carbon and energy flux at the anaplerotic node.

Detailed analyses of the *C. glutamicum*  $\Delta$ *ppc*  $\Delta$ *pyc* mutant evolved to grow on D-glucose revealed the strong up-regulation of a few genes that are under control of the transcriptional regulator RamA. Higher protein abundances were found for the enzymes of the glyoxylate shunt as well as the methylcitrate cycle under solely glycolytic conditions, under which condition the corresponding genes were thought to be repressed. It is inferred that this adaptation must be due to a changed concentration of a metabolite affecting the activity of regulator protein RamA, brought about by a concentration change of the former. This metabolite pool, however, could not be identified from the set of metabolites from glycolysis, TCA cycle and amino acids that was targeted in this study. Since the encoding genes of the altered proteins represent just a small subset of the RamA regulon, it can be concluded that the binding affinities

of RamA to all target genes may be regulated by various effector metabolites and not a single one. Further research, especially based on untargeted metabolomics, will be needed to identify the metabolite regulator(s) active on RamA under D-glucose conditions.

In conjunction with the intracellular metabolomics data we generally conclude that *C. glutamicum* is able to compensate missing carboxylation activities of PEPCx and PCx by activation of the glyoxylate shunt, potentially in combination with the methylcitrate cycle to channel the higher levels of PEP/ pyruvate as well as succinate and thereby also contributing to replenish oxaloacetate. To further substantiate the hypothesis on the reverse operation of the methylcitrate cycle isotope-based metabolic flux analyses with the evolved *C. glutamicum*  $\Delta ppc$   $\Delta pyc$  strain could be conducted in further studies.

Finally, the reproducible effect of bicarbonate formation under excess D-glucose conditions and its consequences for carbon balancing also requires further investigations. For example, a combination of batch experiments under variation of pH and gassing rate as well as thorough modeling of the resulting CO<sub>2</sub>-dynamics in the gas and liquid phase could be an approach for a more accurate determination of CO<sub>2</sub>-formation rates.

## DATA AVAILABILITY STATEMENT

The mass spectrometry proteomics data have been deposited to the ProteomeXchange Consortium via the PRIDE (Perez-Riverol et al., 2019) partner repository with the dataset identifier PXD022622. The reads data of the  $\Delta ppc$   $\Delta pyc$  strain are available in NCBI's SRA via BioProject ID PRJNA678589. The other

datasets generated for this study are available on request to the corresponding author.

## AUTHOR CONTRIBUTIONS

JK and SN designed the research. JK performed data analysis and wrote the manuscript. JK and MP performed the bioreactor cultivations of *C. glutamicum*. BK lysed and digested all samples and performed the LC-MS/MS measurements. JL constructed the *C. glutamicum* double deletion mutants used in this manuscript. TP performed the whole-genome sequencing. SN, TP, and WW revised the manuscript. SN, RT, and BB supervised the research. All authors have given approval to the final version of the manuscript.

## FUNDING

This work was partly funded by the Deutsche Forschungsgemeinschaft (priority program SPP2170, Grant No. 427904493).

## ACKNOWLEDGMENTS

We thank Lothar Eggeling for critical comments on the manuscript.

## SUPPLEMENTARY MATERIAL

The Supplementary Material for this article can be found online at: <https://www.frontiersin.org/articles/10.3389/fbioe.2020.602936/full#supplementary-material>

## REFERENCES

- Auchter, M., Cramer, A., Hüser, A., Rückert, C., Emer, D., Schwarz, P., et al. (2011). RamA and RamB are global transcriptional regulators in *Corynebacterium glutamicum* and control genes for enzymes of the central metabolism. *J. Biotechnol.* 154, 126–139. doi: 10.1016/j.jbiotec.2010.07.001
- Baumgart, M., Unthan, S., Kloß, R., Radek, A., Polen, T., Tenhaef, N., et al. (2018). *Corynebacterium glutamicum* chassis C1\*: building and testing a novel platform host for synthetic biology and industrial biotechnology. *ACS Synth. Biol.* 7, 132–144. doi: 10.1021/acssynbio.7b00261
- Baumgart, M., Unthan, S., Rückert, C., Sivalingam, J., Grünberger, A., Kalinowski, J., et al. (2013). Construction of a prophage-free variant of *Corynebacterium glutamicum* ATCC 13032 for use as a platform strain for basic research and industrial biotechnology. *Appl. Environ. Microbiol.* 79, 6006–6015. doi: 10.1128/AEM.01634-13
- Becker, J., Rohles, C. M., and Wittmann, C. (2018). Metabolically engineered *Corynebacterium glutamicum* for bio-based production of chemicals, fuels, materials, and healthcare products. *Metab. Eng.* 50, 122–141. doi: 10.1016/j.ymben.2018.07.008
- Blombach, B., Buchholz, J., Busche, T., Kalinowski, J., and Takors, R. (2013). Impact of different CO<sub>2</sub>/HCO<sub>3</sub><sup>-</sup> levels on metabolism and regulation in *Corynebacterium glutamicum*. *J. Biotechnol.* 168, 331–340. doi: 10.1016/j.jbiotec.2013.10.005
- Blombach, B., Riester, T., Wieschalka, S., Ziert, C., Youn, J. W., Wendisch, V. F., et al. (2011). *Corynebacterium glutamicum* tailored for efficient isobutanol production. *Appl. Environ. Microbiol.* 77, 3300–3310. doi: 10.1128/AEM.02972-10
- Buchholz, J., Graf, M., Blombach, B., and Takors, R. (2014). Improving the carbon balance of fermentations by total carbon analyses. *Biochem. Eng. J.* 90, 162–169. doi: 10.1016/j.bej.2014.06.007
- Claes, W. A., Pühler, A., and Kalinowski, J. (2002). Identification of two *prpDBC* gene clusters in *Corynebacterium glutamicum* and their involvement in propionate degradation via the 2-methylcitrate cycle. *J. Bacteriol.* 184, 2728–2739. doi: 10.1128/JB.184.10.2728-2739.2002
- Cocaign-Bousquet, M., Guyonvarch, A., and Lindley, N. D. (1996). Growth rate-dependent modulation of carbon flux through central metabolism and the kinetic consequences for glucose-limited chemostat cultures of *Corynebacterium glutamicum*. *Appl. Environ. Microbiol.* 62, 429–436. doi: 10.1128/AEM.62.2.429-436.1996
- Cramer, A., and Eikmanns, B. J. (2007). RamA, the transcriptional regulator of acetate metabolism in *Corynebacterium glutamicum*, is subject to negative autoregulation. *J. Mol. Microbiol. Biotechnol.* 12, 51–59. doi: 10.1159/000096459
- Dalman, T., Dornemann, T., Juhnke, E., Weitzel, M., Wiechert, W., Nöh, K., et al. (2013). Cloud MapReduce for monte carlo bootstrap applied to metabolic flux analysis. *Future Gener. Comp. Sy.* 29, 582–590. doi: 10.1016/j.future.2011.10.007
- Eikmanns, B. J., Thum-Schmitz, N., Eggeling, L., Lüdtke, K.-U., and Sahm, H. (1994). Nucleotide sequence, expression and transcriptional analysis of the *Corynebacterium glutamicum gltA* gene encoding citrate synthase. *Microbiology* 140, 1817–1828. doi: 10.1099/13500872-140-8-1817
- Flamholz, A., Noor, E., Bar-Even, A., and Milo, R. (2012). eQuilibrator—the biochemical thermodynamics calculator. *Nucleic Acids Res.* 40, D770–775. doi: 10.1093/nar/gkr874

- Fränzel, B., Fischer, F., Trötschel, C., Poetsch, A., and Wolters, D. (2009). The two-phase partitioning system—a powerful technique to purify integral membrane proteins of *Corynebacterium glutamicum* for quantitative shotgun analysis. *Proteomics* 9, 2263–2272. doi: 10.1002/pmic.200800766
- Gourdon, P., Baucher, M. F., Lindley, N. D., and Guyonvarc'h, A. (2000). Cloning of the malic enzyme gene from *Corynebacterium glutamicum* and role of the enzyme in lactate metabolism. *Appl. Environ. Microbiol.* 66, 2981–2987. doi: 10.1128/AEM.66.7.2981-2987.2000
- Hünnefeld, M., Persicke, M., Kalinowski, J., and Frunzke, J. (2019). The MarR-type regulator MalR is involved in stress-responsive cell envelope remodeling in *Corynebacterium glutamicum*. *Front. Microbiol.* 10:1039. doi: 10.3389/fmcb.2019.01039
- Jolkver, E., Emer, D., Ballan, S., Kramer, R., Eikmanns, B. J., and Marin, K. (2009). Identification and characterization of a bacterial transport system for the uptake of pyruvate, propionate, and acetate in *Corynebacterium glutamicum*. *J. Bacteriol.* 191, 940–948. doi: 10.1128/JB.01155-08
- Kappelmann, J., Wiechert, W., and Noack, S. (2016). Cutting the gordian knot: identifiability of anaplerotic reactions in *Corynebacterium glutamicum* by means of <sup>13</sup>C-metabolic flux analysis. *Biotechnol. Bioeng.* 113, 661–674. doi: 10.1002/bit.25833
- Klaffl, S., and Eikmanns, B. J. (2010). Genetic and functional analysis of the soluble oxaloacetate decarboxylase from *Corynebacterium glutamicum*. *J. Bacteriol.* 192, 2604–2612. doi: 10.1128/JB.01678-09
- Kogure, T., and Inui, M. (2018). Recent advances in metabolic engineering of *Corynebacterium glutamicum* for bioproduction of value-added aromatic chemicals and natural products. *Appl. Microbiol. Biotechnol.* 102, 8685–8705. doi: 10.1007/s00253-018-9289-6
- Kranz, A., Vogel, A., Degner, U., Kiebler, I., Bott, M., Usadel, B., et al. (2017). High precision genome sequencing of engineered *Gluconobacter oxydans* 621H by combining long nanopore and short accurate illumina reads. *J. Biotechnol.* 258, 197–205. doi: 10.1016/j.jbiotec.2017.04.016
- Krause, J. P., Polen, T., Youn, J. W., Emer, D., Eikmanns, B. J., and Wendisch, V. F. (2012). Regulation of the malic enzyme gene *malE* by the transcriptional regulator MalR in *Corynebacterium glutamicum*. *J. Biotechnol.* 159, 204–215. doi: 10.1016/j.jbiotec.2012.01.003
- Kübler, A., Fränzel, B., Eggeling, L., Polen, T., Wolters, D. A., and Bott, M. (2014). Pupylated proteins in *Corynebacterium glutamicum* revealed by MudPIT analysis. *Proteomics* 14, 1531–1542. doi: 10.1002/pmic.201300531
- Lee, J. H., and Wendisch, V. F. (2017). Production of amino acids - genetic and metabolic engineering approaches. *Bioresour. Technol.* 245, 1575–1587. doi: 10.1016/j.biortech.2017.05.065
- Ma, W. J., Wang, J. L., Li, Y., Yin, L. H., and Wang, X. Y. (2018). Poly(3-hydroxybutyrate-co-3-hydroxyvalerate) co-produced with L-isoleucine in *Corynebacterium glutamicum* WM001. *Microb. Cell Fact* 17:93. doi: 10.1186/s12934-018-0942-7
- Marx, A., De Graaf, A. A., Wiechert, W., Eggeling, L., and Sahm, H. (1996). Determination of the fluxes in the central metabolism of *Corynebacterium glutamicum* by nuclear magnetic resonance spectroscopy combined with metabolite balancing. *Biotechnol. Bioeng.* 49, 111–129. doi: 10.1002/(SICI)1097-0290(19960120)49:2<111::AID-BIT1>3.0.CO;2-T
- Noack, S., Voges, R., Gätgens, J., and Wiechert, W. (2017). The linkage between nutrient supply, intracellular enzyme abundances and bacterial growth: New evidences from the central carbon metabolism of *Corynebacterium glutamicum*. *J. Biotechnol.* 258, 13–24. doi: 10.1016/j.jbiotec.2017.06.407
- Paczia, N., Nilgen, A., Lehmann, T., Gätgens, J., Wiechert, W., and Noack, S. (2012). Extensive exometabolome analysis reveals extended overflow metabolism in various microorganisms. *Microb. Cell Fact* 11:122. doi: 10.1186/1475-2859-11-122
- Perez-Riverol, Y., Csordas, A., Bai, J., Bernal-Llinares, M., Hewapathirana, S., Kundu, D. J., et al. (2019). The PRIDE database and related tools and resources in 2019: improving support for quantification data. *Nucleic Acids Res.* 47, D442–D450. doi: 10.1093/nar/gky1106
- Petersen, S., Mack, C., De Graaf, A. A., Riedel, C., Eikmanns, B. J., and Sahm, H. (2001). Metabolic consequences of altered phosphoenolpyruvate carboxykinase activity in *Corynebacterium glutamicum* reveal anaplerotic regulation mechanisms *in vivo*. *Metab. Eng.* 3, 344–361. doi: 10.1006/mbe.2001.0198
- Peters-Wendisch, P. G., Eikmanns, B. J., Thierbach, G., Bachmann, B., and Sahm, H. (1993). Phosphoenolpyruvate carboxylase in *Corynebacterium glutamicum* is dispensable for growth and lysine production. *FEMS Microbiol. Lett.* 114, 243–243.
- Peters-Wendisch, P. G., Kreutzer, C., Kalinowski, J., Pátek, M., Sahm, H., and Eikmanns, B. J. (1998). Pyruvate carboxylase from *Corynebacterium glutamicum*: characterization, expression and inactivation of the *pyc* gene. *Microbiology* 144, 915–927. doi: 10.1099/00221287-144-4-915
- Peters-Wendisch, P. G., Wendisch, V. F., Degraaf, A. A., Eikmanns, B. J., and Sahm, H. (1996). C-3-carboxylation as an anaplerotic reaction in phosphoenolpyruvate carboxylase-deficient *Corynebacterium glutamicum*. *Arch. Microbiol.* 165, 387–396. doi: 10.1007/s002030050342
- Plassmeier, J., Barsch, A., Persicke, M., Niehaus, K., and Kalinowski, J. (2007). Investigation of central carbon metabolism and the 2-methylcitrate cycle in *Corynebacterium glutamicum* by metabolic profiling using gas chromatography-mass spectrometry. *J. Biotechnol.* 130, 354–363. doi: 10.1016/j.biote.2007.04.026
- Plassmeier, J., Persicke, M., Puhler, A., Sterthoff, C., Ruckert, C., and Kalinowski, J. (2012). Molecular characterization of PrpR, the transcriptional activator of propionate catabolism in *Corynebacterium glutamicum*. *J. Biotechnol.* 159, 1–11. doi: 10.1016/j.jbiotec.2011.09.009
- Riedel, C., Rittmann, D., Dangel, P., Mockel, B., Petersen, S., Sahm, H., et al. (2001). Characterization of the phosphoenolpyruvate carboxykinase gene from *Corynebacterium glutamicum* and significance of the enzyme for growth and amino acid production. *J. Mol. Microbiol. Biotechnol.* 3, 573–583.
- Schwentner, A., Feith, A., Münch, E., Busche, T., Rückert, C., Kalinowski, J., et al. (2018). Metabolic engineering to guide evolution – Creating a novel mode for L-valine production with *Corynebacterium glutamicum*. *Metab. Eng.* 47, 31–41. doi: 10.1016/j.ymben.2018.02.015
- Siegel, D., Permentier, H., Reijngoud, D. J., and Bischoff, R. (2014). Chemical and technical challenges in the analysis of central carbon metabolites by liquid-chromatography mass spectrometry. *J. Chromatogr. B Analyt Technol. Biomed. Life Sci.* 966, 21–33. doi: 10.1016/j.jchromb.2013.11.022
- Stella, R. G., Wiechert, J., Noack, S., and Frunzke, J. (2019). Evolutionary engineering of *Corynebacterium glutamicum*. *Biotechnol. J.* 14:e1800444. doi: 10.1002/biot.201800444
- Tillack, J., Paczia, N., Noh, K., Wiechert, W., and Noack, S. (2012). Error propagation analysis for quantitative intracellular metabolomics. *Metabolites* 2, 1012–1030. doi: 10.3390/metabo2041012
- Trötschel, C., Albaum, S. P., and Poetsch, A. (2013). Proteome turnover in bacteria: current status for *Corynebacterium glutamicum* and related bacteria. *Microb. Biotechnol.* 6, 708–719. doi: 10.1111/1751-7915.12035
- Unthan, S., Baumgart, M., Radek, A., Herbst, M., Siebert, D., Brühl, N., et al. (2015). Chassis organism from *Corynebacterium glutamicum* – a top-down approach to identify and delete irrelevant gene clusters. *Biotechnol. J.* 10, 290–301. doi: 10.1002/biot.201400041
- Unthan, S., Grünberger, A., Van Ooyen, J., Gätgens, J., Heinrich, J., Paczia, N., et al. (2014). Beyond growth rate 0.6: What drives *Corynebacterium glutamicum* to higher growth rates in defined medium. *Biotechnol. Bioeng.* 111, 359–371. doi: 10.1002/bit.25103
- Uy, D., Delaunay, S., Engasser, J. M., and Goergen, J. L. (1999). A method for the determination of pyruvate carboxylase activity during the glutamic acid fermentation with *Corynebacterium glutamicum*. *J. Microbiol. Methods* 39, 91–96. doi: 10.1016/S0167-7012(99)00104-9
- Van Der Rest, M. E., Lange, C., and Molenaar, D. (1999). A heat shock following electroporation induces highly efficient transformation of *Corynebacterium glutamicum* with xenogeneic plasmid DNA. *Appl. Microb. Biotechnol.* 52, 541–545. doi: 10.1007/s002530 051557
- Voges, R., Corsten, S., Wiechert, W., and Noack, S. (2015). Absolute quantification of *Corynebacterium glutamicum* glycolytic and anaplerotic enzymes by QconCAT. *J. Proteomics* 113, 366–377. doi: 10.1016/j.jprot.2014.10.008
- Voges, R., and Noack, S. (2012). Quantification of proteome dynamics in *Corynebacterium glutamicum* by <sup>15</sup>N-labeling and selected reaction monitoring. *J. Proteomics* 75, 2660–2669. doi: 10.1016/j.jprot.2012.03.020
- Wendisch, V. F., Spies, M., Reinscheid, D. J., Schnicke, S., Sahm, H., and Eikmanns, B. J. (1997). Regulation of acetate metabolism in *Corynebacterium*

- glutamicum*: transcriptional control of the isocitrate lyase and malate synthase genes. *Arch. Microbiol.* 168, 262–269. doi: 10.1007/s002030050497
- Zelle, R. M., Harrison, J. C., Pronk, J. T., and Van Maris, A. J. (2011). Anaplerotic role for cytosolic malic enzyme in engineered *Saccharomyces cerevisiae* strains. *Appl. Environ. Microbiol.* 77, 732–738. doi: 10.1128/AEM.02132-10
- Zimmermann, M., Sauer, U., and Zamboni, N. (2014). Quantification and mass isotopomer profiling of alpha-keto acids in central carbon metabolism. *Anal. Chem.* 86, 3232–3237. doi: 10.1021/ac500472c

**Conflict of Interest:** The authors declare that the research was conducted in the absence of any commercial or financial relationships that could be construed as a potential conflict of interest.

Copyright © 2021 Kappelmann, Klein, Papenfuß, Lange, Blombach, Takors, Wiechert, Polen and Noack. This is an open-access article distributed under the terms of the Creative Commons Attribution License (CC BY). The use, distribution or reproduction in other forums is permitted, provided the original author(s) and the copyright owner(s) are credited and that the original publication in this journal is cited, in accordance with accepted academic practice. No use, distribution or reproduction is permitted which does not comply with these terms.